International Journal of Hydrogen Energy 268 (2026) 157081

Contents lists available at ScienceDirect

International Journal of Hydrogen Energy

journal homepage: www.elsevier.com/locate/he

Experimental characterisation of hollow-cone hydrogen jet behaviour under engine-like conditions

Shuo Dong, Yizhuo Feng *, Raghul Nagarajan, Abinash Biswal, Changzhao Jiang, Xinyan Wang, Hua Zhao

Centre for Advanced Powertrain and Fuels, Brunel University of London, UB8 3PH, United Kingdom

ARTICLE INFO

Keywords:
Hydrogen
Hollow-cone jet
Schlieren
Underexpanded jet

ABSTRACT

Internal combustion engines equipped with direct injection (DI) of hydrogen represent a promising pathway toward carbon-neutral transportation. This work presents a systematic experimental investigation of hollow-cone hydrogen jet dynamics generated by an outward-opening injector using high-speed schlieren imaging, integrating jet momentum measurements. The hydrogen jet evolution is identified as a two-stage process, *i.e.*, near-nozzle underexpanded structures dominated by pressure-ratio effects and a subsequent self-similar dense-jet stage governed by momentum. The pressure-ratio-dominant and momentum-dominant scaling laws are evaluated for these two stages, clarifying the governing mechanisms of hollow-cone hydrogen jet development. Furthermore, a quantitative evaluation of hydrogen mixing behaviour is conducted with a constant injected mass under different injection pressures (P_{inj}). The results show that P_{inj} has a limited influence on jet shapes during injection, whereas higher P_{inj} improves spatial mixture homogeneity. The difference in homogeneity can be reduced by allowing a longer mixing time after the end of injection.

Nomenclature

ASOE	After the start of energising
ASOI	After the start of the injection
CVC	Constant volume chamber
DI	Direct injection
EOI	End of injection
GDI	Gasoline direct injection
H_2	Hydrogen
H_2-ICE	Hydrogen internal combustion engines
HC	Hollow-cone
ICE	Internal combustion engine
IMEP	Indicated mean effective pressure
MH	Multi-hole
NI	National Instruments
P_{amb}	Ambient pressure
PDF	Probability density function
PFI	Port fuel injection
P_{inj}	Injection pressure
PR	Pressure ratio
P_s	Penetration
QSS	Quasi-steady state
T_{amb}	Ambient temperature

1. Introduction

Given increasingly stringent global greenhouse gas emissions legislation and environmental policies, the transportation sector faces a significant challenge in decarbonisation. Hydrogen is a flammable gas that can be utilised in internal combustion engines (ICEs) [1,2]. As hydrogen is naturally carbon-free, it is considered a potential alternative fuel, offering a promising solution for reducing CO_2 emissions for ICEs. Experimental studies have demonstrated that hydrogen can be directly used in a conventional internal combustion engine with a slight modification by a port fuel injection (PFI) system [3,4]. However, due to its wide flammable limitation, hydrogen internal combustion engines (H_2-ICEs) with PFI are associated with a high risk of backfire in the intake manifold [5,6]. Furthermore, the loss of volumetric efficiency in PFI leads to significant limitations in engine output and thermal efficiency [7]. Therefore, the direct injection (DI) of hydrogen is considered an attractive technology for high-performance and high-efficiency H_2-ICEs.

Compared with conventional liquid fuels, like gasoline and diesel, hydrogen, as a gaseous fuel, has a significantly lower volumetric heating value, requiring a new injection system to meet engine fuelling and

* Corresponding author.
E-mail address: yizhuo.feng@brunel.ac.uk (Y. Feng).

https://doi.org/10.1016/j.ijhydene.2026.157081
Received 23 May 2026; Received in revised form 11 August 2026; Accepted 13 August 2026
Available online 19 August 2026

packaging requirements. There are two types of injectors for commercial use in the H_2 DI system: multi-hole and hollow-cone injectors [8–10]. Multi-hole (MH) hydrogen injectors, typically employing an inward-lift pintle configuration, offer an axially concentrated cone-shaped hydrogen jet with a dense core along the nozzle axis [11–14]. In comparison, hollow-cone (HC) jets generated by outward-opening injectors form an annular-shaped jet that expands both radially and axially [15]. In general, hollow-cone injectors offer a larger effective flow cross-section, which enables high mass-flow rates under the same injection conditions [16,17]. The annular jet structure promotes rapid radial propagation and mixing with air, resulting in a broader jet area and more homogeneous mixture compared with multi-hole injectors under the same injection conditions [7,10,18]. Furthermore, the outward-opening pintle structure yields a reliable sealing performance, which is critical for H_2-ICEs [17].

Given the fundamental differences between the hollow-cone jet and the conventional multi-hole jet, the hollow-cone jet has attracted increasing research attention, with optical diagnostic techniques widely employed to characterise hydrogen jet behaviour. In a global perspective, the hollow-cone hydrogen jet initially develops with an inward vortex motion, followed by a slight axial expansion [19]. As the jet evolves, the structure progressively contracts toward the centreline, leading to the collapse of the hollow-cone geometry and transition into a more concentrated axial plume. The merged jet subsequently accelerates in the downstream direction, accompanied by a symmetric head vortex, and gradually stabilises into a quasi-steady conical structure. During this evolution, as expected, increasing the pressure ratio significantly enhances axial penetration and enlarges the overall jet area [20–23]. Specifically, for the effect of ambient pressure, Lee et al. [24] indicated that the penetration and jet area decrease as ambient back pressure increases from 0.1 to 3.0 MPa. Moreover, high ambient back pressure will lead to a high drag force, which may prevent the dispersion of hydrogen, and it will further induce a high level of mixture heterogeneity. Based on these findings, the authors suggested either enlarging the injector nozzle angle or operating under lower ambient pressures to facilitate better dispersion and mixing. As for the influence of injection pressure, Coratella et al. [25,26] further investigated hollow-cone hydrogen jets generated by an outward-opening injector using schlieren imaging. The result showed that increasing injection pressure significantly enhances both the axial penetration and radial expansion of the hydrogen jet due to the increased jet momentum and pressure ratio. In the early stage of injection, a stronger radial propagation of the hollow-cone structure was observed under higher injection pressures. However, the intensified radial development simultaneously accelerated the collapse of the hollow-cone jet, leading to an earlier transition into a downstream dense jet. Furthermore, Bae et al. [27] reported that the hydrogen jet penetration and spray angle exhibit strong similarity under the constant pressure ratio, highlighting the dominant role of pressure ratio in governing the evolution of the underexpanded hydrogen jet. Based on these macroscopic hydrogen jet characteristics, the jet morphology is highly sensitive to the operating boundary conditions. Such variations are closely associated with the evolution of near-nozzle compressible flow structures and the subsequent downstream far-field jet development. Therefore, understanding both the near-nozzle underexpanded structures and the far-field jet evolution is essential for clarifying the fundamental development mechanisms of hollow-cone hydrogen jets.

In the near nozzle region, the H_2 jet exhibits an underexpanded structure due to the compressibility under higher pressure ratios. Laichter et al. [10] demonstrated that the under-expanded annular jet exhibited a multiple barrel-shock structure with approximately three shock cells, which dissipated within 10 mm downstream of the nozzle. These shock structures were strongly governed by the pressure ratio, which formed only when the pressure ratio was over 8.5. Besides the pressure ratio, Coratella et al. [28] found that the pintle motion of the outward-opening injector also plays a significant role in the evolution of the near-nozzle structures. The results showed that a Prandtl-Meyer expansion fan is formed when the gaseous hydrogen passes over the pintle surface, and a faster pintle ramp-up can accelerate the initial radial spreading of the jet but also promote its subsequent collapse. Such findings demonstrated that the transient injection process, particularly the evolution of the momentum and pintle motion, plays a critical role in governing the initial dynamics of hollow-cone hydrogen jets [24].

Building on this understanding, the transient momentum characteristics of hydrogen jets have attracted increasing research attention, since the jet momentum directly governs the subsequent jet propagation [29–31]. Based on mass and momentum conservation principles, Bae et al. [27] established a scaling relationship, showing that jet development is positively correlated with the density ratio between the fuel and ambient gas, nozzle exit velocity, nozzle hole diameter, and injection duration. Wang et al. [19] and Wu et al. [32,33] further extended the scaling correlation between hydrogen jet penetration and injection duration by incorporating compressible flow theory and a theoretical injection momentum framework. Their results demonstrated good self-similarity of jet development at the fully developed stage over a wide range of pressure ratios. These findings collectively indicate that injection momentum plays a dominant role in governing hydrogen jet development. However, the above-mentioned studies were predominantly based on the theoretical momentum rather than experimentally measured momentum, leaving uncertainty errors regarding their applicability under real injection conditions.

To address this limitation, the transient momentum characteristics of hydrogen jets can be experimentally quantified using force-sensor-based measurements. Such a method has been widely applied in conventional incompressible liquid fuel injection studies [34]. However, limited research has been conducted on hydrogen. Postrioti et al. [30] presented a momentum flux measurement of hydrogen using a single-hole injector under various pressure ratios in a constant volume vessel. The result demonstrated that the measured momentum is highly sensitive to the sensor position and the sensor target diameters. Specifically, the structure of the Mach disk may reduce the effective momentum when the sensor target is too close to the injector, whereas the momentum is dissipated significantly with a longer measurement distance. In addition, undersized targets would underestimate momentum due to incomplete jet capture, whereas oversized targets were affected by surrounding pressure fields and acoustic oscillations, leading to signal attenuation and spurious fluctuations. As a result, the maximum momentum was observed at distances of 10 mm with a target diameter of 13 mm. Similarly, Peters et al. [35] systematically analysed the sensitivity of the hydrogen jet momentum under various injection conditions with an inward-opening GDI injector. The measured momentum changed due to the sensor target placement. This makes the case of hydrogen injection inherently more complex than that of liquids.

According to the above discussion, the macroscopic morphology, underexpanded flow structures, penetration and mixing characteristics of hollow cone hydrogen jets have been widely investigated. Most of the studies were focused on the global view of the jet. The relationship between injector dynamics and jet development has not been fully understood. Although some research has provided a scaling law for penetration to analyse the governing mechanisms of jet development, previous penetration correlations for hollow-cone hydrogen jets have generally employed momentum estimates based on mass variation in the chamber [19] or theoretical compressible-flow relationships [32], rather than the actual measured jet momentum. Moreover, although pressure ratio and pintle dynamics have been shown to affect the near-nozzle structure, the governing relationships applicable to the near-nozzle compressible structure and downstream jet propagation have not been experimentally distinguished. Finally, the mixing performance under different injection conditions has not been quantitatively evaluated. Therefore, a systematic study linking hydrogen transient momentum evolution, near-nozzle underexpanded structures, far field jet development, and mixing behaviour under varying pressure-ratio conditions is essential. Such understanding will provide valuable guidance for optimising injection strategy in practical H_2-ICEs, ultimately facilitating improved in-cylinder mixture formation.

This work aims to address two key questions: the governing mechanisms and dominant influencing factors for hydrogen jet development, and the relationship between injection conditions and hydrogen mixing characteristics under a specific engine-like condition. In this regard, this study: (i) introduces direct force-based momentum measurements into the analysis of hollow-cone hydrogen jet penetration; (ii) analyses the governing mechanism and provides the scaling law for the pressure-ratio-controlled near-field regime from the measured-momentum-controlled downstream regime; and (iii) examines the role of injection pressure on mixing development under a constant injected hydrogen mass. As above, this work connected injector dynamics, near-nozzle compressible structures, downstream momentum-controlled propagation, and mixing characteristics within an experimental framework.

2. Methods

2.1. Experimental setup

The experiments are designed to systematically characterise the hydrogen injection dynamics of a hollow-cone injector. In particular, a force-based sensor was employed to measure the jet momentum under various conditions. To achieve this, all experiments are performed in an 18 L constant-volume chamber, which provides a well-controlled and optically accessible environment. The experimental setup integrates a high-pressure hydrogen supply system, a synchronised control system, a momentum-based mass flow rate measurement system, and a high-speed Z-type Schlieren imaging system.

The hydrogen is sourced from a 120-bar high-pressure hydrogen cylinder with a pressure regulator to maintain a stable supply pressure. Considering the pressure fluctuation in the fuel rail during the injection period, a high-response pressure transducer with a 200 kHz sample rate is used to measure the instantaneous fuel pressure, mounted at 4 mm downstream of the injector. The captured transient pressure data are subsequently processed using a moving mean filter (window size is 100) to generate a smooth pressure profile for analysis. A medium-pressure, outward-opening hydrogen injector [10,26,28] is employed in this study, operating over an injection pressure range of 20 to 40 bar.

To quantify the local hydrogen transient momentum flux, a high-sensitivity piezo-electric force transducer (Kistler type 9215A, 0-20 N) is employed. The sensor is equipped with a bespoke 12 mm diameter target plate and positioned at a standoff distance of 4 mm below the injection. The 4 mm stand-off distance was selected to reduce the direct influence of the supersonic core, while remaining sufficiently close to minimise momentum losses caused by jet spreading and turbulent dissipation before impingement [14,36,37]. The 12 mm target diameter was subsequently selected based on the radial extent of the hollow-cone jet observed in the near-field Schlieren images, as shown in Fig. 1. Each measurement sequence consisted of 10 consecutive injections into the constant-volume chamber. To ensure statistical reliability and eliminate stochastic fluctuations, this process was repeated for 10 independent sets, and a sufficient dwell time was allowed to cool back down to room temperature and pressure stabilisation between each set, ensuring the gas reached a stable quiescent state at room temperature. As a result, the actual hydrogen jet momentum is equal to the measured force, *i.e.*, $\dot{M} = F_z$ [38,39].

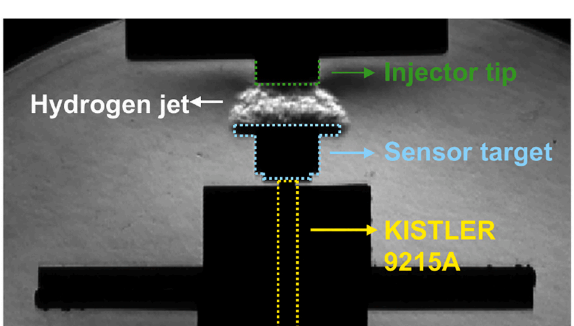

Fig. 1. Experimental setup for the momentum flux measurements.

The injection is driven by a National Instruments (NI) cRIO-9066 controller, integrating an NI 9751 module for injection driving and an NI 9411 module for digital signal acquisition. The synchronisation between the injector driver, camera, and pressure sensors is achieved through TTL pulse generation via a custom LabVIEW-based control interface. Fig. 2 provides an illustration of the driven signal and measurement results.

The macroscopic jet characteristics, including Mach disk formation and jet evolution behaviour, are obtained from the Schlieren technique. The illustration of the Schlieren experiment testbench is shown in Fig. 3. The high-speed Z-type Schlieren system is arranged with a 1.5 W 460 nm LED light source (LMS-460), two parabolic mirrors with a diameter of 192 mm (Edmund, $\lambda/8$, $f = 1016$ mm), and a precision adjustable rectangle aperture (OWIS-SP60). The collimated light beam passed through the parallel 150 mm diameter optical windows of the chamber. The gas density gradient, governed by the Gladstone-Dale relation, is captured with a high-speed camera (Photron NOVA S9) at 24,000 fps. The resulting image dimension is 384 × 768 pixels, yielding an approximate physical image resolution of 0.167 mm per pixel. It should be noted that the sensitivity of a Schlieren system is fundamentally determined by the orientation of the knife-edge relative to the refractive index gradients. Considering the complex underexpanded hydrogen jet structure near the nozzle, where density gradients occur simultaneously in both axial and radial directions, the system utilised a specialised aperture employing a combined half-horizontal and half-vertical knife-edge cutting technique. By implementing this "corner-cut" configuration, the system becomes sensitive to the density gradients along both axes. Furthermore, to ensure the reliability and reproducibility of the Schlieren image and to accurately capture the fine-scale flow structures, each injection condition is repeated five times.

2.2. Experimental conditions

Following the description of the experimental setup, the hydrogen jet was investigated in the chamber under engine-like conditions, which represent a similar thermodynamic condition to that of the light-duty DI hydrogen engine. Table 1 summarises the specific operating conditions in this study. The injection pressure varies from 20 to 40 bar, while the ambient backpressure is adjusted to achieve pressure ratios, $PR = P_{inj}/P_{amb}$, ranging from 5 to 20. The ambient temperature within the test

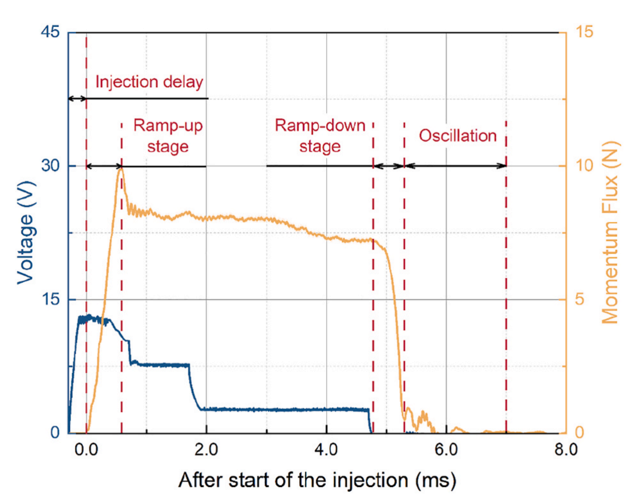

Fig. 2. Illustration of the injector-driven signal and measurement recording.

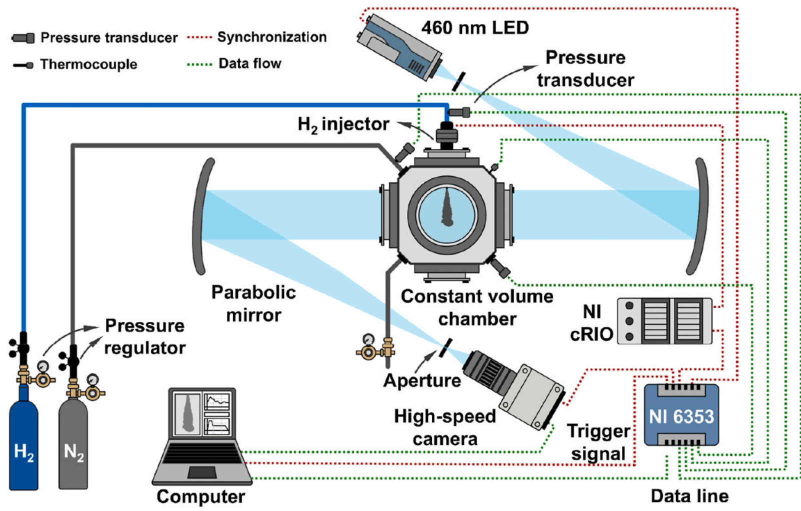

Fig. 3. Schematic of the Z-type Schlieren system for hollow cone hydrogen jets.

Table 1
Experimental conditions.

Description		Value
Ambient conditions	Filling gas	100% N_2
	Ambient temperature (K)	291
	Ambient pressure (bar)	1 to 5
Injection conditions	Test fuel	H_2
	Injection pressure (bar)	20, 30, 40
	Pressure ratio ($PR = P_{inj}/P_{amb}$)	5, 10, 15, 20
	Injection duration (ms)	1, 2, 3, 4, 5

chamber is isothermally maintained at 291 K. Prior to each test case and between consecutive injection events, a strict purging protocol is implemented to ensure a controlled thermodynamic environment and eliminate residual fuel accumulation. Specifically, the chamber is thoroughly purged and subsequently pressurised with high-purity nitrogen to the target chamber backpressure.

Considering the high molecular diffusivity of hydrogen, the mixing is governed not only by the turbulence induced by injection, but also by the molecular diffusion driven by the concentration gradients. To evaluate the mixing performance under an engine-like condition, we further conducted a set of experiments employing the same injection mass with various injection pressures. As shown in Table 2, the injection mass is 5 mg, corresponding to a mid-load operating condition for a light-duty H_2-ICE, based on our previous experiment [40,41]. The injection pressure is tested, ranging from 20 to 40 bar, resulting in the injection duration shortened from 1.30 ms to 0.69 ms, respectively.

2.3. Schlieren image post-processing

To quantitatively characterise the transient jet morphology, the image post-processing algorithm is developed and implemented in MATLAB, as shown in Fig. 4.

For each frame, background subtraction and image enhancement are first applied to improve the contrast of the image. The Otsu algorithm is then used to convert the grayscale image into a binary mask by using adaptive thresholds [42]. A scaled Otsu threshold of 0.8 is applied to retain faint jet features, followed by a minimum area constraint to remove background noise. The jet boundary is subsequently extracted using morphological operations and Canny edge detection, illustrated in Fig. 4(b). Finally, the hydrogen jet penetration is defined as the axial distance from the injector tip to the furthest downstream point of the projected jet contour, as shown in Fig. 4(d).

Table 2
Jet behaviour under the same injection mass.

Injection pressure (bar)	Injection duration (ms)	Injected mass (mg/ per injection)	Ambient pressure (bar)
20	1.38	5	2, 5
30	0.92		2, 5
40	0.69		2, 5

3. Results and discussion

3.1. Global view of the transient hollow-cone hydrogen jet

Fig. 5 illustrates the transient evolution of hydrogen jets from the start of injection to the quasi-steady stage under pressure ratios of 5, 10, and 15, corresponding to combinations of injection pressures (20 and 30 bar) and ambient pressures (2, 3, and 4 bar).

The transient jet evolution is similar across different pressure ratio conditions. In the initial stage, the jet generates an inward vortex, subsequently leading to the collapse of the hollow-cone structure. Then, the jet propagates rapidly downstream and approaches a quasi-steady, self-similar development. To better illustrate jet development, we also prepared a video of the Schlieren results for the different injection conditions as supplementary material.

It should be noted that the near-nozzle Mach disk structure shows a significant dependence on pressure ratio, and the Mach disk can only be clearly observed in the Schlieren image when PR is over 5. In addition, the near-nozzle structure and jet development exhibit a similarity under the same PR, as shown in the second and third rows of Fig. 5, while the penetration of the jet is significantly prolonged when increasing the injection pressure or decreasing the ambient pressure, due to the higher injection momentum. Considering the two-stage jet characteristics, the near-nozzle shock structures and the far-field jet penetration are further discussed in detail in the following sections.

3.2. Near nozzle Mach disk structure

To analyse the near nozzle jet behaviour, the post-processing workflow quantifies the microscopic shock structures. Considering the stochastic fluctuations inherent in turbulent jets, ensemble averaging is performed using five repeated time-resolved images at identical time steps. The Mach-disk positions correspond to the local minima in the centreline intensity profile. Fig. 6 illustrates the ensemble-averaged Schlieren visualisation, highlighting the characteristic of near-nozzle

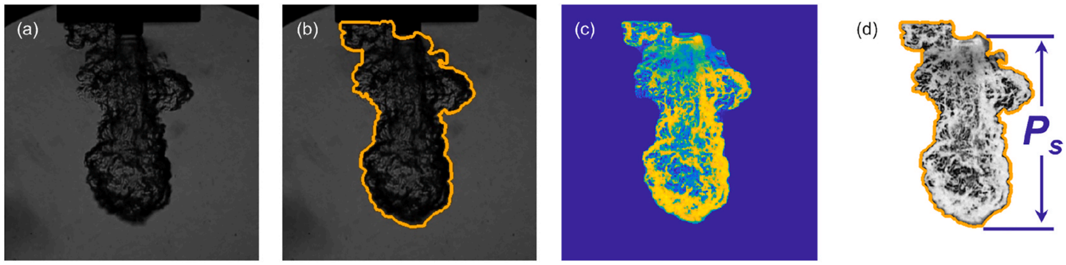

Fig. 4. Example of the post-processing for jet Schlieren image: (a) original image; (b) jet boundary; (c) normalised image intensity; (d) definition of the jet penetration (P_S).

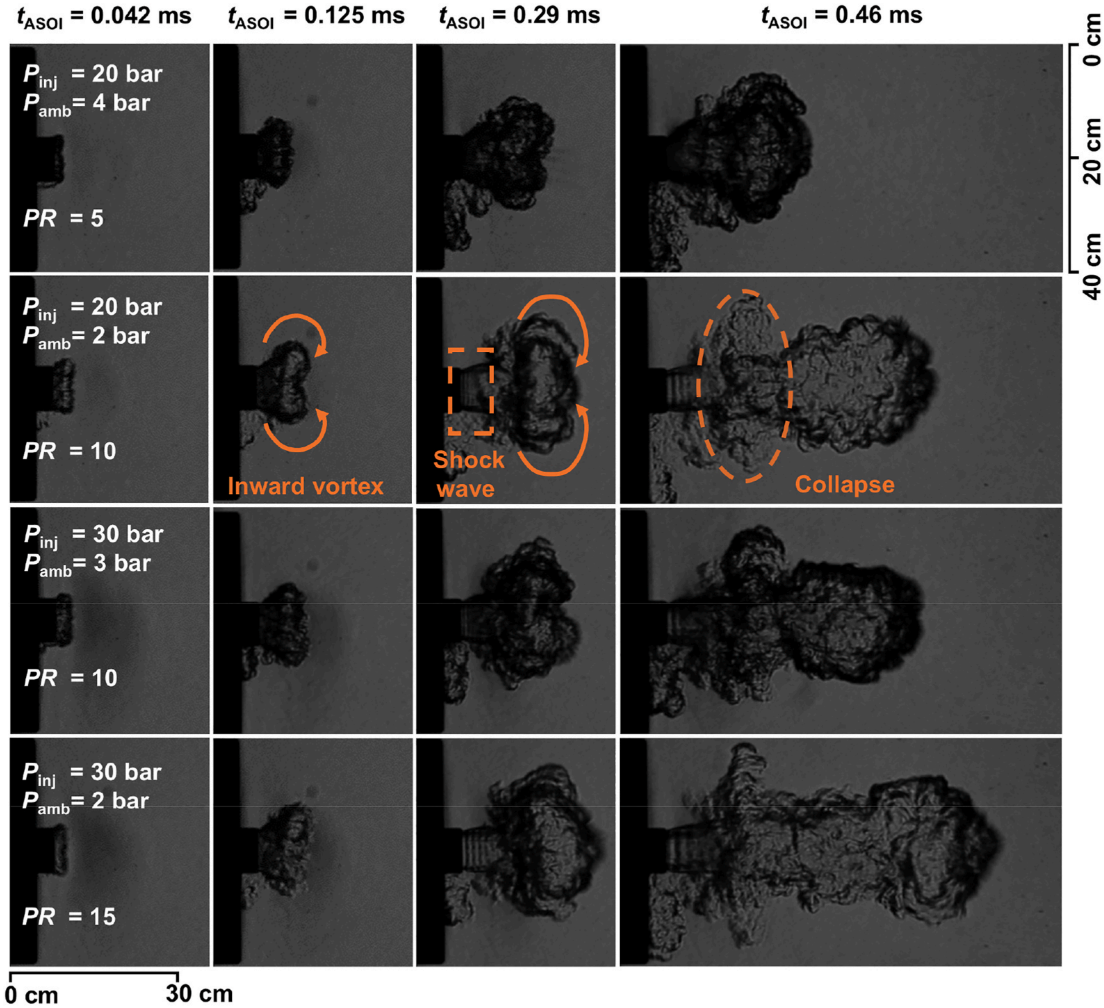

Fig. 5. Temporal evolution of the hydrogen jet under various injection pressure and ambient pressure conditions.

barrel shock structures.

Based on the post-processing of the intensity profile, the temporal evolution of the Mach disk positions is quantified in Fig. 7. As shown in Fig. 7(a), the distance between the Mach disk and the nozzle tip increased first, then dropped slightly, and finally stabilised during the late-stage injection. Temporally, the under-expanded structure can be clearly identified in Schlieren images after approximately 0.2 to 0.3 ms ASOI and becomes stable after about 0.65 ms ASOI for all injection conditions. The maximum distances of both the first and second Mach disks occur at approximately 0.55 ms ASOI, consistent with the peak timing of momentum, which demonstrates that the formation of the underexpanded structure is driven by the pintle motion. Spatially, under the same pressure ratio, the Mach disk positions show almost no variation with changes in injection/back pressures. Fig. 7(b) further presents the quasi-steady state (QSS) height of Mach disks. The QSS Mach disk is normalised by the effective orifice diameter D_e, *i.e.*, the nondimensional location H/D_e. The results indicate that the nondimensional location of Mach disks exhibits a linear dependence on the pressure ratio, which can be expressed by the linear fitting curve of $H_{First}/D_e = 0.39682\ (P_{inj}/P_{amb})^{0.5}$-0.87083 and $H_{Second}/D_e = 0.74263\ (P_{inj}/P_{amb})^{0.5}$-1.52429 for the first and second Mach disks, respectively. These results indicate that the underexpanded structures in the near field of the hollow-cone jet are governed by the pressure ratio.

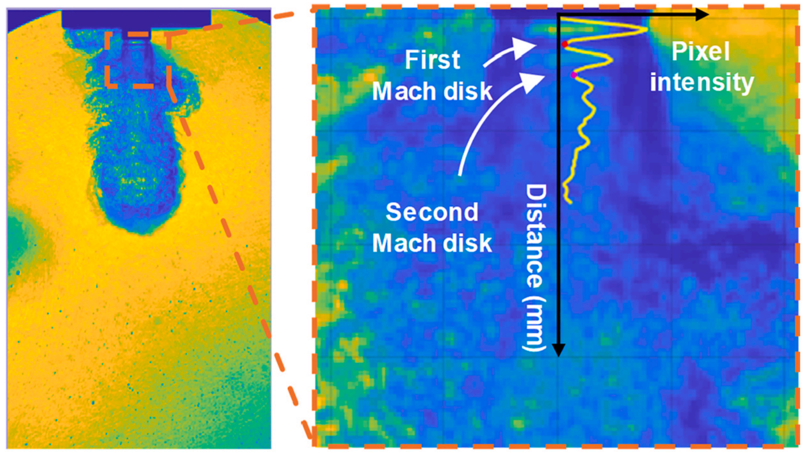

Fig. 6. Determination of the Mach disk location in the hydrogen jet light-intensity images.

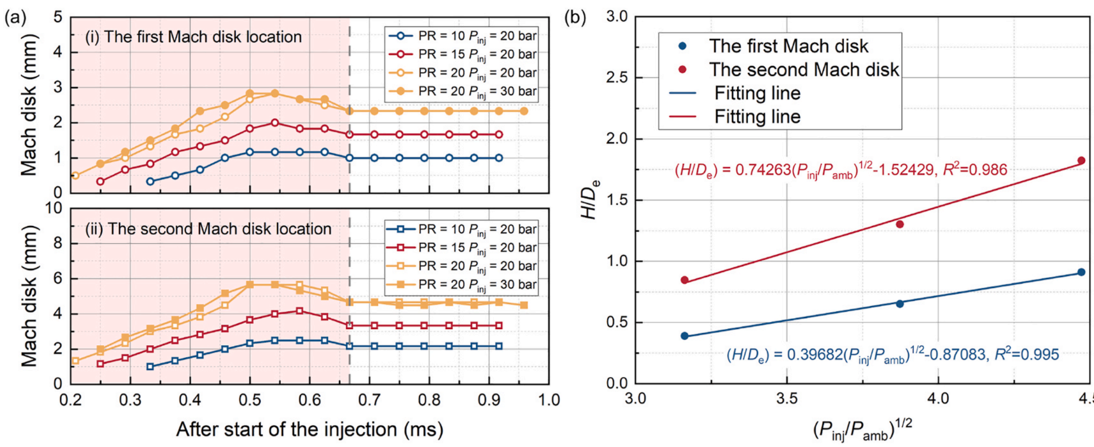

Fig. 7. Mach disk characteristics: (a) Mach disk locations under various injection conditions; (b) quasi-steady state non-dimensional Mach disk positions as a function of the pressure ratios.

3.3. Self-similar jet development

Fig. 8(a) exhibits the jet penetration under various injection pressure and ambient pressure conditions. The penetration shows a two-stage development. At the early stage of the injection, the penetration development is slow, governed by the formation of the near-nozzle underexpanded structure. After the jet collapsed, the hydrogen moves downward as a dense jet, and the transient jet velocity is significantly increased compared to the early stage. Specifically, the jet development shows a self-similar behaviour under the same pressure ratio.

The previous studies have shown that the gaseous jet penetration can be scaled by the jet momentum and ambient density [43], *i.e.*, $y \sim (\dot{M}/\rho_{\mathrm{amb}})^{0.25}\, t^{0.5}$. Fig. 8(b) shows the scaled penetration by using the mean quasi-steady measured jet momentum plotted against $t^{0.5}$. For each operating condition, the momentum signals from 100 repeated injections were ensemble-averaged, and the mean momentum was subsequently calculated over the quasi-steady stage, *i.e.*, after the ramp-up stage and before the ramp-down stage shown in Fig. 2. Based

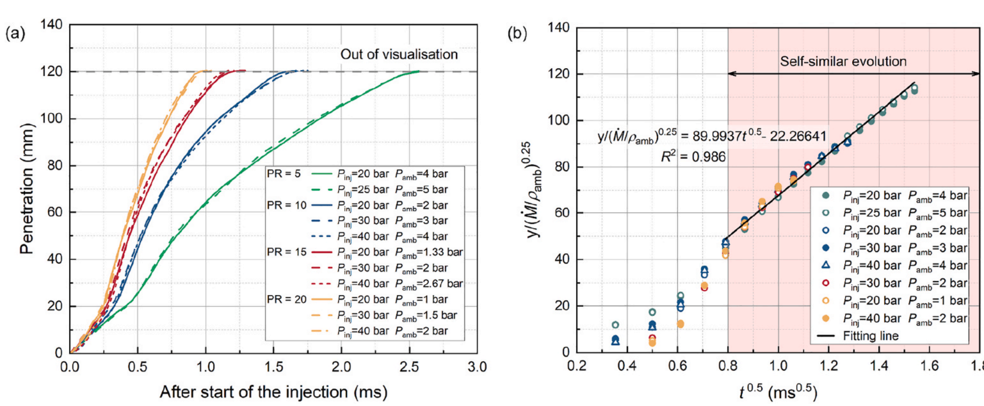

Fig. 8. (a) Hydrogen jet penetration under different pressure ratios (b) Self-similar scaling of normalised hydrogen jet.

on the measured results, the mean relative standard deviation of the measured penetration ranges from 1.60%~4.49%. And the relative standard deviation of the momentum term in the scaling law ($\dot{M}^{0.25}$) corresponds to approximately 0.15%~0.34%. The small random uncertainty confirms the convergence of the penetration scaling law. As shown in Fig. 8(b), the scaled penetration converges into a universal linear fitting line after approximately $t^{0.5} = 0.8$, following the scaling law of $y/(\dot{M}/\rho_{amb})^{0.25}\bullet = 89.9937t^{0.5}$ - 22.2664. The corresponding transition time point (*i.e.*, $t = 0.64$ ms, as shown in Fig. 7) closely coincides with the formation period of the QSS underexpanded structure. This indicates that the second stage of the jet development establishes a self-similar behaviour driven by the jet momentum. As discussed in Section 3.2, the early stage of the jet development, corresponding to the formation of underexpanded structures, is primarily controlled by the pressure ratio. Therefore, during this period, the penetration does not follow the momentum-based scaling law. However, Wu et al. [32] reported that both the first and second stages of the hollow-cone jet penetration can be linearly scaled with $(\dot{M}/\rho_{amb})^{0.25}\,t^{0.5}$ using a different slope. This difference can be attributed to two main factors: first, there is no obvious Mach disk structure in the presented Schlieren results from Wu et al. [32]; second, the scaling law proposed in that study was derived using theoretical jet momentum rather than experimentally measured momentum, which significantly deviates from the actual jet momentum.

In addition, the result in Fig. 8(b) demonstrates that the jet operating at higher pressure ratios reaches the universal scaling line earlier. This suggests that a stronger momentum flux accelerates the collapse of the initial hollow-cone structure, thereby facilitating an earlier transition to the momentum-controlled turbulent jet development.

Based on the discussion above, Fig. 9 illustrates a conceptual model of the hollow-cone hydrogen jet. In contrast to the solid-cone jet, the hollow-cone jet exhibits a two-stage characteristic. Specifically, the near-nozzle region is dominated by the pressure-ratio, characterised by a hollow-cone underexpanded structure when PR exceeds 5. The formation of the near-nozzle structure is directly governed by the motion of the injector pintle. Once the hollow-cone structure collapses, the jet transitions into the self-similar development region, where a momentum-dominated downstream dense jet becomes the primary factor governing jet penetration.

The proposed two-stage model is expected to be a general qualitative physical framework to underexpanded gaseous jets generated by outward-opening hollow-cone injectors. Nevertheless, quantitative characteristics, such as the fitting coefficients of the scaling laws, of both stages remain dependent on injector geometry and operating conditions. Specifically, in the first stage, although the Mach disk position generally follows $H/D_e \sim (P_{inj}/P_{amb})^{0.5}$, the pressure-ratio threshold and development time of the Mach disk, as well as the fitting coefficients, can be affected by the pintle angle, annular flow area, nozzle geometry, and pintle motion [26,28]. Similarly, the proportionality coefficient of the penetration scaling $y \sim (\dot{M}/\rho_{amb})^{0.25}\,t^{0.5}$ may also vary with injector

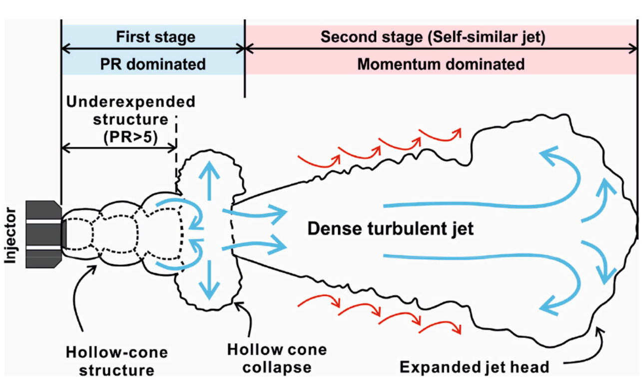

Fig. 9. The conceptual model for the hollow-cone hydrogen jet.

configuration, such as the pintle angle [26] and pintle motion characteristics [32]. Therefore, the scaling forms may be transferable between similar injector types, whereas their quantitative coefficients and transition characteristics require injector-specific calibration. Further validation is also required at higher ambient pressures and temperatures beyond the present range of 1–5 bar and 291 K.

3.4. *Effect of injection pressure at constant injection mass*

While the aforementioned two-stage hydrogen dynamics defines the basic free jet behaviours, it is essential to evaluate how these characteristics develop in the practical engine operating conditions. Considering that the molecular diffusivity of hydrogen is significantly higher than that of conventional fossil fuels, hydrogen can diffuse rapidly in the cylinder, and the mixing process can be controlled synergistically by the turbulent transportation and molecular diffusion. In this regard, we would like to further evaluate the role of injection pressure by investigating the jet characteristics and mixing performance under various injection pressures with constant injection mass, as detailed in Table 2. To be specific, the injection mass is selected as 5 mg, corresponding to a medium load condition for a light-duty SI hydrogen engine [40,41]. Therefore, the injection duration is reduced from 1.38 ms at 20 bar to 0.69 ms at 40 bar. In addition, the experiments are conducted under 2 bar and 5 bar ambient pressure, corresponding to early injection and late injection timings in the engine, respectively. This strategy allows for a direct comparison of the mixing characteristics under an engine-like condition.

Fig. 10 presents the evolution of the hydrogen jet. As shown in Fig. 10(a), both the injection pressure and ambient pressure have a significant influence on jet penetration. However, the penetration shows no obvious decay after the end of injection. Considering the momentum-dependent characteristic of the jet evolution, Fig. 10(b) further compares the penetration using a non-dimensional time (t^*). The non-dimensional time is defined as

$$t^* = t_{ASOI}/t_d \quad (1)$$

where t_{ASOI} is the physical time after the start of injection, and t_d is the injection duration. It can be found that, for a given ambient pressure, the penetration profiles corresponding to different injection pressures tend to converge into a single curve plotted against the non-dimensional time, although slight differences exist during the early stages of jet development associated with the formation of underexpanded structures.

Fig. 11 further exhibits the jet boundary contours at the time of the end of injection (EOI) for 20 bar, 30 bar, and 40 bar injection pressure under two different ambient pressures. All five repetition results for each condition have been presented in the figure. Consistent with the conclusion of the penetration, the jet angles, as well as the jet boundary contours, also show a high similarity for different injection pressures at the EOI. Such results suggest that, in practical engine applications, a similar jet penetration and jet contour can be achieved by increasing the injection duration while using a lower injection pressure.

Considering that Schlieren images represent spatial gradients of gas density, the level of homogeneity of the mixture can be qualitatively evaluated using the normalised intensity [24,44]. It should be noted that the normalised Schlieren intensity is used here only as a qualitative and comparative indicator of the evolution of the projected density-gradient non-uniformity. Schlieren imaging responds to line-of-sight-integrated refractive-index gradients, which are related to gas-density gradients through the Gladstone-Dale relationship, rather than directly to the local hydrogen concentration. Therefore, the normalised intensity PDF is used here as a comparative indicator under identical optical configurations, ambient conditions and image-processing procedures. A distribution concentrated toward lower normalised intensities represents weaker projected density gradients and hence a more homogeneous mixture,

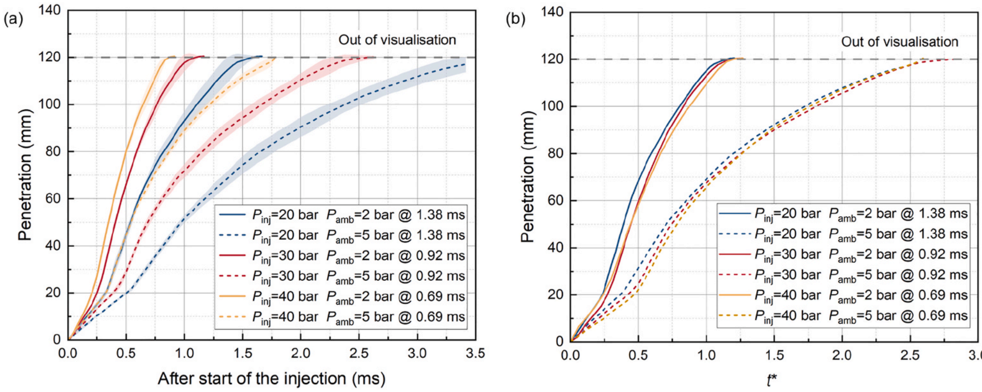

Fig. 10. (a) Hydrogen penetrations at the same injection mass; (b) Hydrogen injection patterns against the non-dimensional time ($t^* = t_{ASOI}/t_d$).

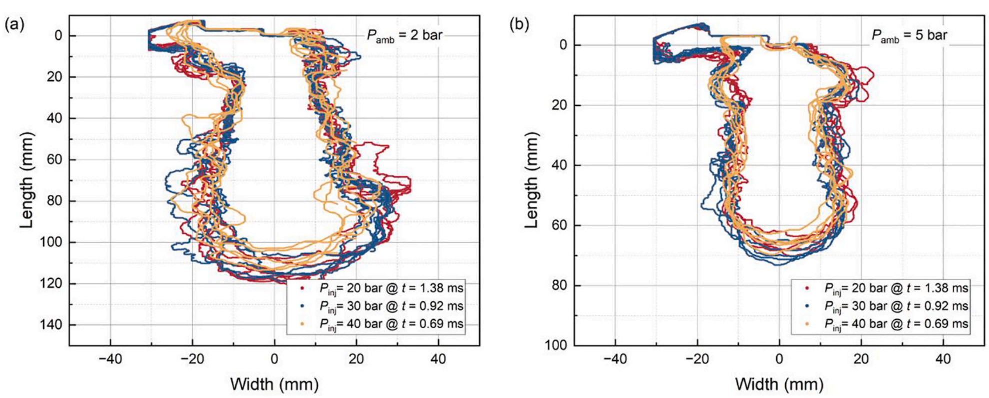

Fig. 11. Hydrogen jet contours with the same injection mass under (a) $P_{amb} = 2$ bar and (b) $P_{amb} = 5$ bar at EOI timing, corresponding to 1.38 ms for $P_{inj} = 20$ bar, 0.92 ms for $P_{inj} = 30$ bar, and 0.69 ms for $P_{inj} = 40$ bar.

whereas higher and more broadly distributed intensities indicate stronger mixture stratification.

Fig. 12 presents the ensemble-average Pseudo-colour Schlieren images and the probability density functions (PDFs) of the normalised

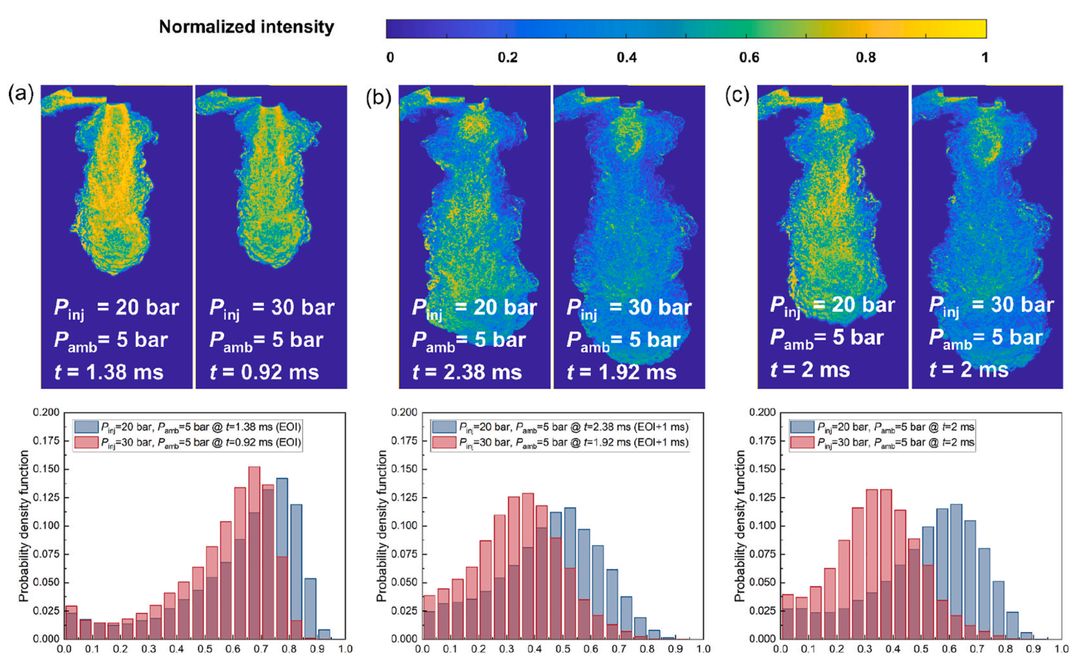

Fig. 12. Evolution of the hydrogen jet mixing under $P_{amb} = 5$ bar with $P_{inj} = 20$ bar and $P_{inj} = 30$ bar, respectively. (a) End of the injection timing, corresponding to 1.38 ms for $P_{inj} = 20$ bar and 0.92 ms for $P_{inj} = 30$ bar; (b) 1 ms after the end of the injection timing, corresponding to 2.38 ms for $P_{inj} = 20$ bar and 1.92 ms for $P_{inj} = 30$ bar; and (c) 2 ms after the start of the injection, corresponding to 3.38 ms for $P_{inj} = 20$ bar and 2.92 ms for $P_{inj} = 30$ bar.

intensity for $P_{inj} = 20$ bar and $P_{inj} = 30$ bar under $P_{amb} = 5$ bar at different timings, respectively.

As shown in Fig. 12(a), the overall jet boundaries at the end of injection are similar for both injection pressure conditions. However, the normalised intensity distributions exhibit noticeable differences. Specifically, the inner region of the jet shows a high-density gradient in $P_{inj} = 20$ bar, indicating strong heterogeneity in the mixing, which is consistent with the result of the intensity PDFs. Fig. 12(b) further compares the mixing performance at 1 ms after EOI, corresponding to $t = 2.38$ ms for $P_{inj} = 20$ bar and $t = 1.92$ ms for $P_{inj} = 30$ bar, namely the same relative mixing time after EOI. The PDF results indicate that the intensity decreases significantly for both injection pressures, representing the diffusion of hydrogen within the chamber. However, after the same diffusion time, the mixture of $P_{inj} = 30$ bar still exhibits more homogeneity than that of $P_{inj} = 20$ bar. For reference, Fig. 12(c) shows the Schlieren results and corresponding intensity PDFs distribution at $t = 2$ ms. By comparing the results in Fig. 12(b) and (c), it can be observed that a longer mixing time reduces the difference in mixing homogeneity between the low and high injection pressure cases.

The above results demonstrate that, although the macroscopic boundaries of the jet are similar at EOI timing across different injection pressures for a fixed injected mass, the subsequent mixing quality is different. A higher injection pressure always yields a better homogeneity of the mixture (narrower distribution). Nevertheless, due to the high molecular diffusivity of hydrogen, a longer mixing time may improve the homogeneity under a low injection pressure condition. This suggests that, under a practical engine operating condition, comparable mixing quality may be achieved at lower injection pressures by employing earlier injection timing to allow sufficient mixing time. In contrast, late direct injection strategies require higher injection pressures to ensure adequate mixture homogeneity.

4. Conclusions

This study systematically investigated the momentum, near-nozzle structure, downstream penetration and post injection mixing behaviour characteristics of a hollow-cone hydrogen jet under various injection pressure and ambient backpressure conditions. The main conclusions are summarised as follows.

➢ The development of the hollow-cone hydrogen jet can be described using two stage-dependent governing relationships. The initial near-nozzle region is governed primarily by the pressure ratio, whereas the downstream self-similar dense jet is governed by the measured axial momentum and ambient density. Within the initial phase, the jet exhibits an underexpanded structure with an inward vortex, which entrains toward the jet axis. When the pintle reaches the maximum lift, the initial hollow-cone structure collapses and develops downstream, leading to the second-stage self-similar jet.

➢ In the first stage of the jet, the Mach disk can be clearly identified near the nozzle when the pressure ratio exceeds 5. During the formation of the Mach disk, the positions of both the first and second Mach disks increase initially, followed by a slight decrease before stabilising. The stabilised position shows an approximately linear dependence on $(P_{inj}/P_{amb})^{0.5}$. Notably, the time at which the Mach disk reaches its maximum axial distance coincides with the peak of the ROI. This observation indicates that the temporal formation and evolution of the Mach disks are closely governed by the pintle ramp-up motion.

➢ Once the initial hollow-cone structure collapses, the jet penetration follows a momentum-based scaling law governed by the force sensor measured momentum and ambient density, *i.e.*, $y \sim (\dot{M}/\rho_{amb})^{0.25} t^{0.5}$. The transition to this relationship occurs at approximately 0.64 ms, coinciding with the establishment of the quasi-steady under-expanded structure. However, jets at higher pressure ratios reach the universal scaling earlier, indicating that increased PR accelerates hollow-cone collapse and facilitates an earlier transition to momentum-controlled turbulent jet development.

➢ The hydrogen mixing performance is finally assessed with a fixed injected hydrogen mass under different injection pressures, representing a specific mid-load engine condition. The results reveal that, although the overall jet penetration and jet boundaries at the end of injection remain similar for different injection pressures, the spatial homogeneity of the mixture can be improved by using a higher injection pressure. However, the difference in mixing homogeneity between the low and high injection pressures can be potentially minimised by employing a longer mixing time after EOI, due to the high molecular diffusive coefficient of hydrogen.

CRediT authorship contribution statement

Shuo Dong: Formal analysis, Investigation, Methodology, Visualization, Writing – original draft. **Yizhuo Feng:** Formal analysis, Investigation, Methodology, Visualization, Writing – review & editing. **Raghul Nagarajan:** Investigation. **Abinash Biswal:** Investigation. **Changzhao Jiang:** Funding acquisition. **Xinyan Wang:** Funding acquisition, Supervision, Writing – review & editing. **Hua Zhao:** Conceptualization, Funding acquisition, Supervision, Writing – review & editing.

Declaration of competing interests

The authors declare that they have no known competing financial interests or personal relationships that could have appeared to influence the work reported in this paper.

Acknowledgements

This work is supported by an EPSRC Prosperity Partnership Grant (UKRI562) and a UKRI Future Leaders Fellowship (UKRI1057). Authors would also like to acknowledge the support of PHINIA and CMB Tech, and technical support by Andrew Selway, Eamon Wyse, Abin Mathew and Enshen Lu.

Appendix A. Supplementary data

Supplementary data to this article can be found online at https://doi.org/10.1016/j.ijhydene.2026.157081.

References

[1] Agarwal AK, Mounaïm-Rousselle C, Brequigny P, Dhar A, Hespel C, Patel C, et al. Future of internal combustion engines using sustainable, scalable, and storable E-fuels and biofuels for decarbonizing transport and enabling advanced combustion technologies. Prog Energy Combust Sci 2025;110:101236.
[2] Verhelst S, Wallner T. Hydrogen-fueled internal combustion engines. Prog Energy Combust Sci 2009;35:490–527.
[3] Kiesgen G, Klüting M, Bock C, Fischer H. The new 12-cylinder hydrogen engine in the 7 series: the H2 ICE age has begun, Detroit. United States: Michigan; 2006. 2006-01–0431.
[4] Mohamed M, Zaman Z, Lu E, Feng Y, Wang X, Zhao H. Experimental investigation of performance and emission characteristics of a diesel light-duty engine fuelled with pure hydrogen. Stuttgart, Germany. 2025. 2025-01–0314.
[5] Gao J, Wang X, Song P, Tian G, Ma C. Review of the backfire occurrences and control strategies for port hydrogen injection internal combustion engines. Fuel 2022;307:121553.
[6] Khalid AH, Muhamad Said MF, Veza I, Abas MA, Roslan MF, Abubakar S, et al. Hydrogen port fuel injection: review of fuel injection control strategies to mitigate backfire in internal combustion engine fuelled with hydrogen. Int J Hydrog Energy 2024;66:571–81.
[7] Dober G, Dober G, Hoffmann G, Doradoux L, et al. Direct injection systems for hydrogen engines. MTZ Worldw 2021;82:60–5. n.d.
[8] Salazar VM, Kaiser SA. An optical study of mixture preparation in a hydrogen-fueled engine with direct injection using different nozzle designs. SAE Int J Engines 2009;2:119–31.
[9] Yip HL, Srna A, Liu X, Kook S, Hawkes ER, Chan QN. Visualization of hydrogen jet evolution and combustion under simulated direct-injection compression-ignition engine conditions. Int J Hydrog Energy 2020;45:32562–78.

[10] Laichter J, Kaiser SA, Rajasegar R, Srna A. Optical investigation of mixture formation in a hydrogen-fueled heavy-duty engine with direct-injection. SAE Int. J. Adv. & Curr. Prac. in Mobilit 2023;6(2):593–612.
[11] Peña Fernández JJ, Sesterhenn J. Compressible starting jet: pinch-off and vortex ring–trailing jet interaction. J Fluid Mech 2017;817:560–89.
[12] Dong S, Shi H, Zhang G, Feng Y, Lu E, Wang X, et al. Transient helium jet evolution using high speed schlieren imaging. Florence, Italy. 2025. 2025-32–0057.
[13] Zhang Z, Yuan Y, Yang X, Yang F, Shi C, Wang X. Experimental study on the development characteristics of the extremely under-expanded hydrogen jet structure for high pressure direct injection hydrogen engines. Energy 2026;359: 141499.
[14] Hamzehloo A, Aleiferis PG. Gas dynamics and flow characteristics of highly turbulent under-expanded hydrogen and methane jets under various nozzle pressure ratios and ambient pressures. Int J Hydrog Energy 2016;41:6544–66.
[15] Sankesh D, Petersen P, Lappas P. Flow characteristics of natural-gas from an outward-opening nozzle for direct injection engines. Fuel 2018;218:188–202.
[16] Dober G, Hoffmann G, Doradoux L, et al. Direct injection systems for hydrogen engines. 2021.
[17] Dober G, Piock WF, Meissonnier G, Hoffmann G. Hydrogen injection systems - a smart path to zero CO2 powertrains. MTZ Worldw 2022;84:28–35.
[18] Houidi MB, Moreno-Cabezas K, Zaihi A, Aljohani B, Wu H, AlRamadan A, et al. Investigating hydrogen direct injection technology: a comparative analysis of nozzle geometries for enhanced mixing in internal combustion engines. Proc Combust Inst 2024;40:105631.
[19] Wang X, Sun B, Luo Q, Bao L, Su J, Liu J, et al. Visualization research on hydrogen jet characteristics of an outward-opening injector for direct injection hydrogen engines. Fuel 2020;280:118710.
[20] Im HG, Liu X, Ben Houidi M, Wu H, Zaihi A, Moreno-Cabezas K, et al. Toward H2 ICE: experimental and computational characterization of hydrogen injection, mixing, and combustion. Int J Engine Res 2025:14680874251353371.
[21] Peters M, Maes N, Dam N, Van Oijen J. Characterizing and visualizing the direct injection of hydrogen into high-pressure argon and nitrogen environments. Int J Hydrog Energy 2024;66:304–15.
[22] Hu C, Hu L, Chen H, Li L, Wu Z, Deng J. Hydrogen jet characteristics of an outward-opening injector based on schlieren imaging. South Korea: Busan; 2025. 2025-01–0228.
[23] Payri R, Novella R, Nasser KI, Bori-Fabra O. Spray characterization of direct hydrogen injection as a green fuel with lower emissions. Energies 2024;17:2405.
[24] Lee S, Kim G, Bae C. Behavior of hydrogen hollow-cone spray depending on the ambient pressure. Int J Hydrog Energy 2021;46:4538–54.
[25] Coratella C, Tinchon A, Hespel C, Dober G, Foucher F. Experimental investigation of the comparison between helium and hydrogen jets exiting a DI outward-opening injector via schlieren technique. Capri, Italy. 2025. 2025-24–0068.
[26] Coratella C, Tinchon A, Oung R, Doradoux L, Foucher F. Experimental investigation of the combined impact of backpressure with the pintle dynamic on the hydrogen spray exiting a medium pressure DI outward-opening injector. Int J Hydrog Energy 2024;49:432–49.
[27] Bae G, Lee J, Moon S. Transient development and structure of supersonic gas jets from narrow-cone-angle pintle-type hydrogen injector. Fuel 2025;384:134072.
[28] Coratella C, Tinchon A, Oung R, Doradoux L, Dober G, Hespel C, et al. Experimental characterization of a hydrogen hollow cone jet at under-expanded conditions via schlieren technique. Int J Hydrog Energy 2024;72:730–43.
[29] Yeganeh M, Akram MS, Cheng Q, Karimkashi S, Kaario O, Larmi M. Experimental study of hydrogen jet dynamics: investigating free momentum and impingement phenomena. Int J Hydrog Energy 2024;68:1423–37.
[30] Postrioti L, Martino M, Fontanesi S, Breda S, Magnani M. Experimental and numerical momentum flux analysis of jets from a hydrogen injector. Detroit, Michigan, United States. 2024. 2024-01–2616.
[31] Kuensch ZA, Schlatter S, Keskinen K, Hulkkonen T, Larmi M, Boulouchos K. Experimental investigation on the gas jet behavior for a hollow cone piezoelectric injector. 2014. 2014-01–2749.
[32] Wu H, Ben Houidi M, Almatrafi F, Wu B, Du J, Magnotti G, et al. Hydrogen jet characteristics with an outwardly opening piezo injector. Phys Fluids 2025;37: 036103.
[33] Wu H, Silva M, Houidi MB, Almatrafi F, Wu B, Cenker E, et al. Experimental characterization of a high-flow hydrogen injector with four-hole jet-forming cap. Fuel 2026;405:136619.
[34] Payri R, Bracho G, Soriano JA, Fernández-Yáñez P, Armas O. Nozzle rate of injection estimation from hole to hole momentum flux data with different fossil and renewable fuels. Fuel 2020;279:118404.
[35] Peters M, Maes N, Dam N, Van Oijen J. A framework to characterize the flow of high-pressure hydrogen injectors. Exp Therm Fluid Sci 2026;170:111576.
[36] Wilkes Inman J, Danehy P, Nowak R, Alderfer D. Fluorescence imaging study of impinging underexpanded jets. In: 46th AIAA Aerosp. Sci. Meet. Exhib. Reno, Nevada: American Institute of Aeronautics and Astronautics; 2008.
[37] Anaclerio G, Capurso T, Torresi M. Gas-dynamic and mixing analysis of under-expanded hydrogen jets: effect of the cross section shape. J Fluid Mech 2023;970: A8.
[38] Payri R, Garcia J, Salvador F, Gimeno J. Using spray momentum flux measurements to understand the influence of diesel nozzle geometry on spray characteristics. Fuel 2005;84:551–61.
[39] Pickett LM, Manin J, Payri R, Bardi M, Gimeno J. Transient rate of injection effects on spray development. 2013. 2013-24–0001.
[40] Mohamed M, Feng Y, Wang X, Zhao H, Hall J. Investigating the impact of compression ratio on hydrogen combustion and emission: an experimental analysis. Int J Engine Res 2025:14680874251341641.
[41] Mohamed M, Biswal A, Wang X, Zhao H, Hall J. Experimental investigation for enhancing the performance of hydrogen direct injection compared to gasoline in spark ignition engine through valve timings and overlap optimization. Fuel 2024; 372:132257.
[42] Otsu N. A threshold selection method from gray-level histograms. IEEE Trans Syst Man Cybern 1979;9:62–6.
[43] Ouellette P, Hill PG. Turbulent transient gas injections. J Fluid Eng 2000;122: 743–52.
[44] Chun K, Ratvasky W, Lee C, Locke R. Focused schlieren flow visualization studies of multiple venturi fuel injectors in a high pressure combustor. In: 32nd Aerosp. Sci. Meet. Exhib. Reno,NV,U.S.A.: American Institute of Aeronautics and Astronautics; 1994.